Ecological Modelling 273 (2014) 63–78

Contents lists available at ScienceDirect

Ecological Modelling

journal homepage: www.elsevier.com/locate/ecolmodel

Coupling 3-D Eulerian bio-physics (ROMS) with individual-based shellfish ecophysiology (SHELL-E): A hybrid model for carrying capacity and environmental impacts of bivalve aquaculture☆

Diego A. Ibarra*, Katja Fennel, John J. Cullen

Department of Oceanography, Dalhousie University, Halifax, Nova Scotia, PO BOX 15000, B3H 4R2, Canada

ARTICLE INFO

Article history:
Received 28 January 2013
Accepted 21 October 2013

Keywords:
Bivalve aquaculture
Carrying capacity
Nutrient dynamics
Shellfish ecophysiology
Ecosystem modelling

ABSTRACT

As bivalve aquaculture continues to grow, it is imperative to understand the spatially-explicit interactions between farmed bivalves and the environment. However, the ability of models to represent a large number of bivalve ecophysiology and environmental variables—in 3-D spatially-explicit domains—has been limited by computational constraints. To overcome some of these computational limitations, we developed an optimized hybrid model by two-way coupling a state-of-the-art Eulerian model (Regional Ocean Modeling System; ROMS) that simulates physical, planktonic and sediment dynamics, with an individual-based model (IBM) that simulates shellfish ecophysiology (SHELL-E). The IBM model efficiently represents sparsely-distributed variables that do not occur in every grid cell of the domain, and simplifies the representation of complex life-history and physiological processes, like spawning events. We applied the hybrid model to a mussel farm in Ship Harbour (Eastern Canada) and compared model results against measurements of physical variables, water samples (chlorophyll, nutrients, oxygen and suspended sediments) and mussel size distributions. The hybrid model reproduced the main dynamics of the physical, planktonic and sediment Eulerian variables, as well as the bivalve ecophysiology IBM variables. Prognostic limitations estimated by the model suggested that mussels were temperature-stressed during parts of the summer, and food-limited during parts of the winter. We also used the hybrid model to estimate the production carrying capacity of the farm and we found that the farm is not overstocked. However, we also found that the estimation of carrying capacity strongly depends on the inferred natural mortality, which is difficult to estimate accurately. This work aims to transfer sound and open-source oceanographic tools (i.e. ROMS) into the applied fields of aquaculture research and management.

1. Introduction

Bivalve aquaculture is growing exponentially worldwide, representing about 65% of total marine aquaculture production and about 11% of total seafood produced for human consumption (statistics for 2009; FAO, 2010). If this industry is to expand in a sustainable manner, it is imperative to understand and quantify the effect of farmed bivalves on the environment, as well as the influence of environmental conditions on the production of bivalves. This implies that bivalve aquaculture models must include a two-way coupling scheme between bivalves and the environment, to adequately resolve the relevant feedbacks.

Following the expansion of bivalve aquaculture, the development of models that represent bivalve-environment interactions has also been growing rapidly during the last three decades (e.g. Incze et al., 1981; Fréchette et al., 1989; Dowd, 2003; Bacher and Gangnery, 2006; Grant et al., 2008; Grangeré et al., 2010). Although these models have diverse foci and approaches, they all fall into two basic categories: (1) Eulerian or grid-based models, or (2) individual-based models.

Eulerian or grid-based models track variables inside fixed volumes of space (i.e. boxes or grid cells). They are the model of choice to simulate variables that behave like tracers (e.g. temperature, phytoplankton concentration, etc.), where a single average value represents the state inside a whole box or grid cell (Lande and Lewis, 1989), and where exchanges among boxes or grid cells, along with changes within the box, are used to represent the dynamics everywhere within the gridded model domain. Eulerian models are by far the most commonly used models representing bivalve-environment interactions. The first models described the interactive influences of bivalve filtration and water currents on the concentration of phytoplankton in 1-D horizontal (Incze et al.,

* Corresponding author. Tel.: +1 902 494 3557; fax: +1 902 494 3877.
E-mail addresses: Diego.Ibarra@dal.ca (D.A. Ibarra), Katja.Fennel@dal.ca (K. Fennel), John.Cullen@dal.ca (J.J. Cullen).

0304-3800/$ – see front matter © 2013 Authors. Published by Elsevier B.V. All rights reserved.
http://dx.doi.org/10.1016/j.ecolmodel.2013.10.024

1981; Rosland et al., 2011) and vertical (Fréchette et al., 1989; Duarte et al., 2008) scenarios. Later models also included primary productivity and other lower-trophic level dynamics; however, a single box (i.e. 0-D model) was used to represent an entire bay (e.g. Dowd, 1997; Dame and Prins, 1998). Some newer studies used an individual growth model forced with environmental data (Bourles et al., 2009; Rosland et al., 2009). Meanwhile, the spatial resolution of other bivalve-environment models has increased over the years from 2-D box models (Grant et al., 2007; Troost et al., 2010), to 2-D models with fine grids (Duarte et al., 2003; Grant et al., 2008; Grangeré et al., 2010; Guyondet et al., 2010), to fine grids in 3-D (Marinov et al., 2007; Spillman et al., 2008; Leon et al., 2011, this study). These bivalve-environment models can use different physiology sub-models; for example, some estimate bivalve growth using Scope-For-Growth sub-models (SFG; Bayne et al., 1976), while others use Dynamic Energy Budget theory (DEB; Kooijman, 1986, 2000, 2010). However, all these models use the Eulerian framework, with domains divided in boxes or grid cells, and with variables representing the average state in each box or cell. Bivalves inside grid cells are also represented as an average concentration; however, unlike conventional Eulerian tracers (e.g. plankton concentration or temperature), the concentration of bivalves is not subject to transport by advection and turbulent diffusion processes. Moreover, if the Eulerian model is designed with many size-classes, each class would be defined with its own state variable. For bivalves to grow from one size-class to the next one, at each time-step some mass has to be subtracted from the smaller class and added to the larger class.

Individual-based models (IBMs; Grimm and Railsback, 2005) track variables associated with sparsely distributed particles, each representing an individual (e.g. a bivalve) or a group of identical individuals. Commonly, 2-D and 3-D individual-based models are used to study larval dynamics (fish larvae: see review by Miller, 2007; bivalve larvae: North et al., 2008, 2010). The majority of these IBM models are forced with output from an Eulerian bio-physical model (i.e. one-way coupling), allowing the particles (each representing an individual larva) to "drift around", thereby experiencing different environmental conditions, like temperature, plankton concentration, etc. In bivalve aquaculture, individual particles have been used to represent individual bivalves seeded in different shellfish growing areas (e.g. Ferreira et al., 2008); as each particle encounters different environmental conditions, the variables tracked for each particle (e.g. bivalve biomass and bivalve size) also evolved differently, depending on its surroundings. At the end of the simulation, the variables tracked for all particles are used to compute the properties of the system (e.g. total bivalve biomass, or evolution of size in a particular area). This is why, in IBM models, the system properties are said to "emerge" from the properties of the individual particles (Grimm and Railsback, 2005). However, it is important to emphasize that—although one-way coupled IBM models are very useful to assess the impact of the environment on individuals—the reverse is not possible. That is, the model structure of conventional one-way coupled IBM models does not allow individuals to influence the variables of the Eulerian model in which they are embedded; for example, bivalves cannot change the concentration of phytoplankton.

Individual-based models have not been used extensively in studies of bivalve aquaculture. In addition to the study by Ferreira et al. (2008) mentioned above, there are a few examples of their use in 0-D applications (e.g. Bacher and Gangnery, 2006), and as a method for parameter optimization (Duarte et al., 2010).

Here, we utilize a type of model referred to as an Eulerian/IBM hybrid (Ibarra, 2011). Such hybrids simultaneously operate two models: an Eulerian model describes the dynamics of physical and planktonic ecosystem variables that are defined everywhere within a gridded domain (e.g. currents, temperature, nutrients, plankton, detritus, etc.), while an IBM model describes the dynamics of variables only defined at discrete locations that are sparsely distributed within the domain (e.g. bivalve biomass, size, assimilation rates, etc.). The Eulerian and IBM models run simultaneously and are two-way coupled, thus allowing Eulerian variables to modify IBM variables and vice-versa. Mass is exchanged among variables in the two models, and total mass is conserved in the system. The structure of hybrid models allow feedbacks between bivalves and the environment, thus enabling bivalves to alter the environment as the same time the environment modifies bivalve physiology. Additionally, because bivalve equations are only computed at some discrete locations (i.e. instead of in every grid cell within the domain), hybrid models can represent numerous bivalve ecophysiology variables, in a 3-D high-resolution domain, without compromising model speed.

The objectives of this study are to (1) develop a hybrid Eulerian/IBM model capable of resolving spatially variable interactions and feedbacks between planktonic ecosystem variables and aquacultured bivalves, (2) assess model performance by applying the hybrid model to a fjord in Eastern Canada containing mussel aquaculture, and then comparing model results against available data, (3) estimate the production carrying capacity of the mussel farm, (4) evaluate the role of natural mortality of bivalves on the estimation of production carrying capacity, and (5) highlight the advantages of hybrid models in the fields of aquaculture research and management.

2. Materials and methods

2.1. Model overview

We implemented the shellfish ecophysiology model, SHELL-E, in the Regional Ocean Modeling System (ROMS), which is a state-of-the-art, open-source, 3-D ocean model (Haidvogel et al., 2008; http://myroms.org). Within ROMS, we used the main hydrodynamic module, the sediment transport module (Warner et al., 2008), one of the lower-trophic biological modules (Fennel et al., 2006), and the individual-based biological module (Ibarra, 2011). The hydrodynamic, planktonic ecosystem and sediment transport models operate under an Eulerian or grid-based framework (i.e. model domain is discredited into a grid). The individual-based biological module operates in a particle-based framework (Ibarra, 2011), where many particles can be inserted at discrete locations anywhere within the model domain. In this study, each particle represents a separate Culture Unit, each containing a number of identical bivalves (Fig. 1). Model details and equations are provided as online supplemental material; symbols and units are presented in Table 1. Below we only provide a brief summary of the model functioning.

In the model, each bivalve filters particles from the water-column (i.e. phytoplankton, zooplankton and detritus) at a rate controlled by the environmental variables experienced within the grid cell, such as temperature, salinity and oxygen concentration. The environmental control on bivalve filtration is imposed via limiting functions (e.g. Fig. 2). Some of the material filtered by the bivalves is incorporated as bivalve somatic tissue, some is incorporated as gonads, and some is returned to the water column as waste (faeces, pseudofaeces and ammonia). Additionally, gonads are emptied during spawning events, which occur when the gonads reach a threshold fraction of the total weight. Bivalves are also subject to natural mortality and harvesting. The water-column variables and the bivalve variables are mass-balanced, therefore any change in bivalve mass causes a corresponding and inverse change of mass in the water-column variables (with the exception harvesting, where harvested biomass is assumed to exit the system). The two-way coupling between the Eulerian planktonic ecosystem

Table 1
List of variables, parameters and other symbols used in this study. Note that model equations are provided as online supplemental material.

Symbol	Units	Value (Reference)	Description
(i) Coordinates and indices			
j	dimensionless	(Eq. 2–1 in 1)	Eulerian scalar index
k	dimensionless	(Eq. 2–3 in 1)	Culture Unit index
t	s (or d)	(Eq. 2–1 in 1)	Time
x	m	(Eq. 2–1 in 1)	Horizontal coordinate in the East-West direction
y	m	(Eq. 2–1 in 1)	Horizontal coordinate in the North-South direction
σ	dimensionless	(Eq. 2–1 in 1)	Vertical sigma coordinate
(ii) State variables			
Hydrodynamic model			
$Temp$	°C	(2)	Local temperature
$Salt$	dimensionless	(2)	Local salinity
u	$m\,s^{-1}$	(2)	Mean component of the velocity in the x direction
v	$m\,s^{-1}$	(2)	Mean component of the velocity in the y direction
Θ	s^{-1}	(2)	Mean component of the velocity in the vertical (σ) direction
Planktonic ecosystem model			
Chl	$mg\,Chl\,m^{-3}$	(Eq. 9 in 3)	Local concentration of chlorophyll
$LDet$	$mmol\,N\,m^{-3}$	(Eq. 12 in 3)	Local concentration of large detritus
NO_3	$mmol\,N\,m^{-3}$	(Eq. 13 in 3)	Local concentration of nitrate
NH_4	$mmol\,N\,m^{-3}$	(Eq. 14 in 3)	Local concentration of ammonium
Phy	$mmol\,N\,m^{-3}$	(Eq. 1 in 3)	Local concentration of phytoplankton
Oxy	$mmol\,O_2\,m^{-3}$	(19)	Local concentration of oxygen
$SDet$	$mmol\,N\,m^{-3}$	(Eq. 11 in 3)	Local concentration of small detritus
Zoo	$mmol\,N\,m^{-3}$	(Eq. 10 in 3)	Local concentration of zooplankton
Sediment transport model			
Sed	$g\,m^{-3}$	(Eq. 5 in 5)	Local concentration of inorganic sediments
Shellfish ecophysiology (SHELL-E) model			
$Gonad_k$	$mmol\,N\,ind^{-1}$	Eq. 12	Reproductive biomass of an individual bivalve in Culture Unit k
$Soma_k$	$mmol\,N\,ind^{-1}$	Eq. 11	Structural biomass of an individual bivalve in Culture Unit k
n_k	ind	Eq. 17	Number of individual bivalves in Culture Unit k
(iii) Other ancillary and diagnostic variables and functions			
Hydrodynamic model			
H_z	m	(2)	Thickness of the grid cell
Planktonic ecosystem model			
I	$W\,m^{-2}$	(Eq. 5 in 3)	Photosynthetically available radiation
Shellfish ecophysiology (SHELL-E) model			
Bivalves			
A_k	$mmol\,N\,ind^{-1}\,d^{-1}$	Eq. 3	Assimilation rate of an individual bivalve in Culture Unit k
B_k	$mmol\,N\,ind^{-1}$	Eq. 2	Biomass of an individual bivalve in Culture Unit k
F_k	$m^3\,ind^{-1}\,d^{-1}$	Eq. 4	Filtration rate of an individual bivalve in Culture Unit k
F_k^{max}	$m^3\,ind^{-1}\,d^{-1}$	Eq. 4	Maximum filtration rate of an individual bivalve in Culture Unit k
Fae_k	$mmol\,N\,ind^{-1}\,d^{-1}$	Eq. 15	Faeces production rate of an individual bivalve in Culture Unit k
$Food$	$mmol\,N\,m^{-3}$	$Phy + Zoo + SDet$	Local concentration of food
$Harvest_k$	$ind\,d^{-1}$	Eq. 18	Number of individual bivalves removed from a Culture Unit in a time step through harvesting
$PsFae_k$	$mmol\,N\,ind^{-1}\,d^{-1}$	Eq. 16	Pseudofaeces production rate of an individual bivalve in Culture Unit k
$Spawning_k$	$mmol\,N\,ind^{-1}\,d^{-1}$	Eq. 14	Biomass of gametes expelled during reproduction by an individual bivalve in Culture Unit k
R_k	$mmol\,N\,ind^{-1}\,d^{-1}$	Eq. 10	Respiration rate of an individual bivalve in Culture Unit k
RE_k	Dimensionless	Eq. 13	Reproductive effort (i.e. fraction of production allocated to reproduction) of an individual bivalve in Culture Unit k
$f_k(Temp)$	Dimensionless	Eq. 6	Functional response of bivalve filtration to temperature
$f_k(Salt)$	Dimensionless	Eq. 7	Functional response of bivalve filtration to salinity
$f_k(Food)$	Dimensionless	Eq. 9	Functional response of bivalve filtration to food (i.e. plankton + zooplankton + detritus)
$f_k(Oxy)$	Dimensionless	Eq. 8	Functional response of bivalve filtration to oxygen
(iv) Parameters			
Hydrodynamic model			
K_ψ	$m^2\,s^{-1}$	(2)	Eddy diffusivity coefficient
υ_θ	$m^2\,s^{-1}$	(2)	Tracer kinematic diffusivity
Planktonic ecosystem model. Same as in Fennel et al. (2006), except for the parameters below			
K_P	$(mmol\,N\,m^{-3})^2$	(3)	Half-saturation concentration of phytoplankton ingestion by zooplankton
κ_{CDOM}	m^{-1}	(4)	Diffuse attenuation coefficient for downwelling PAR irradiance due to CDOM
κ_{TOTAL}	m^{-1}	(4)	Total diffuse attenuation coefficient for downwelling PAR irradiance
g_{max}	$(mmol\,N\,m^{-3})^{-1}\,d^{-1}$	0.75 (22)	Maximum grazing rate of phytoplankton by zooplankton

Table 1 (*Continued*)

Symbol	Units	Value (Reference)	Description
n_{max}	d^{-1}	0.072 (22)	Phytoplankton mortality
m_P	d^{-1}	0.01 (22)	Maximum nitrification rate
θ_{max}	mg Chl (mg C)$^{-1}$	0.15 (22)	Maximum ratio of chlorophyll to phytoplankton C
Shellfish ecophysiology (SHELL-E) model			
AE_P	Dimensionless	0.9 (6)	Absorption efficiency of bivalves on phytoplankton
AE_D	Dimensionless	0.2 (6)	Absorption efficiency of bivalves on small detritus
AE_Z	Dimensionless	0.3 (7)	Absorption efficiency of bivalves on zooplankton
B_{Pub}	mmol N ind^{-1}	0.43 (8)	Bivalve biomass at puberty
B_{ref}	mmol N ind^{-1}	1 (Eq. 5)	Biomass of a reference bivalve
F_{ref}^{max}	m^3 ind^{-1} d^{-1}	0.025 (22)	Filtration rate exhibited by a reference bivalve, B_{ref}, when evaluated in ideal environmental conditions
GT	Dimensionless	0.44 (21)	Threshold fraction (i.e. $Gonad_k/B_k$) triggering spawning
K_{Temp}^H	(°C)$^{-1}$	0.1 (10)	Decreasing coefficient for limitation due to temperature at upper boundary
K_{Temp}^L	(°C)$^{-1}$	0.5 (10)	Decreasing coefficient for limitation due to temperature at lower boundary
K_{Salt}^L	(PSU)$^{-1}$	0.25 (11)	Decreasing coefficient for limitation due to salinity at lower boundary
K_{Oxy}^L	(mmol O_2 m^{-3})$^{-1}$	0.02 (13)	Decreasing coefficient for limitation due to oxygen at lower boundary
K_{Food}	mmol N m^{-3}	1 (7)	Half-saturation food concentration for bivalve filtration
K_{RE}	mmol N ind^{-1}	0.86 (12)	Half-saturation constant for reproductive effort, RE_k
NOQ	mol N (mol O_2)$^{-1}$	0.01 (18)	Nitrogen:oxygen quotient for bivalve respiration
Oxy_L	mmol O_2 m^{-3}	17.5 (13)	Lower limit of tolerance range for oxygen
R_m	d^{-1}	0.002 (22)	Weight-specific maintenance respiration rate of an individual bivalve
$Salt_L$	PSU	10 (11)	Lower limit of tolerance range for salinity
$Temp_H$	°C	25 (9)	Upper limit of tolerance range for temperature
$Temp_L$	°C	−4 (10)	Lower limit of tolerance range for temperature
β	Dimensionless	0.12 (6)	Cost of growth coefficient of an individual bivalve
ε_P	Dimensionless	1 (7)	Filtration efficiency of bivalves on phytoplankton
ε_D	Dimensionless	0.5 (7)	Filtration efficiency of bivalves on small detritus
ε_Z	Dimensionless	0.3 (7)	Filtration efficiency of bivalves on zooplankton
λ^{Nat}	d^{-1}	0.00137(20)	Natural mortality rate of bivalves in Culture Unit k
λ^{Harv}	d^{-1}	0.001 (16)	Harvesting rate
(v) Other			
Ψ^j	Vary		State of the jth Eulerian tracer (e.g. temperature, sediment concentration or phytoplankton concentration)
D_Ψ	Vary		Horizontal diffusivity terms
C_{Eul}^j	Vary		Eulerian source/sink terms for the jth Eulerian scalar
C_{IBM}^j	vary		Individual-based source/sink terms for the jth Eulerian scalar

1 Ibarra (2011).
2 Haidvogel et al. (2008).
3 Fennel et al. (2006).
4 See text in Section 1.3 in online supplemental material.
5 Warner et al. (2008).
6 Grant et al. (2008).
7 Guyondet et al. (2010).
8 Bayne et al. (1983).
9 Gonzalez and Yevich (1976).
10 Calculated to yield less than 10% limitation at 0 °C and 30% limitation at 15 °C (Thompson, 1984).
11 Calculated based on lethal salinity of 10 PSU and 10% limitation at 22.5 PSU (Almada-Villela, 1984).
12 Calculated to yield a maximum mussel size of approximately 100 mm (Ibarra, 2003).
13 Calculated to stop filtration at 17.5 mmol O_2 m^{-3} and to cause a 5% limitation at 175 mmol O_2 m^{-3} (Wang and Widdows, 1993).
14 Kooijman (2000).
15 Wallentinus (1984).
16 pers. comm. (J. Stairs, 2011).
17 Lotze et al. (1999).
18 Widdows and Johnson (1988).
19 Fennel et al. (2013).
20 Estimated so that, at the end of the one-year simulation, the final total biomass of bivalves in the embayment was the same as the initial total biomass.
21 Estimated from mussel meat yields (Smith et al., 2009), where maximum observed yields correspond to mussel with full gonad and minimum yields correspond to mussels with empty gonads.
22 Tuned.

model and the individual-based bivalve physiology model allows for the simultaneous computations of (1) the effect of the environment on bivalves and (2) the effect of bivalves on the environment.

2.2. Model application

We applied the coupled model to Ship Harbour, Nova Scotia, Eastern Canada (Fig. 3), which is an estuarine fjord with a mussel farm (see farm details in Section 2.3). We compared model results with observations, however the modelling period (2004–2005) was different than the period of collection of the observations, because we did not have boundary forcing for the time when samples were collected (water samples: 1988–1992; CTD and currents: 2001; mussel size-distributions: 2001). Also, we compared our model results against published data from other sites in Atlantic Canada, including Mahone Bay and Bedford Basin, Nova Scotia (Cranford

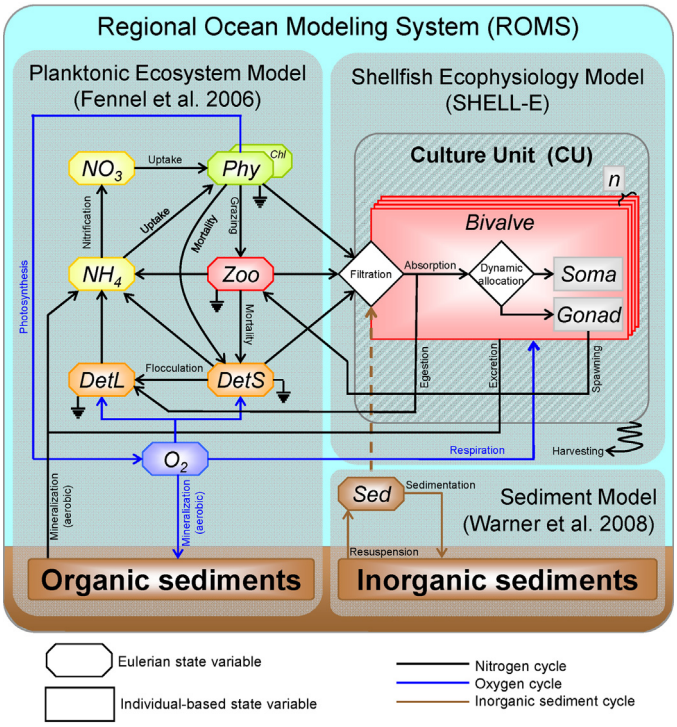

Fig. 1. Diagram of the hybrid Eulerian/IBM model used in this study.

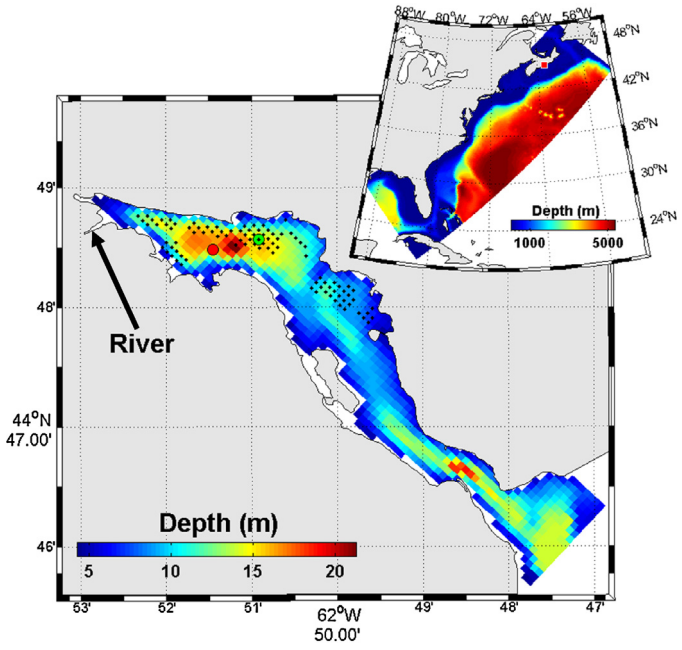

Fig. 3. Upper-right corner shows bathymetry of the larger model domain (North-East North American shelf), which was used to force the open boundary of the smaller model domain (Ship Harbour, Eastern Canada), marked in the larger domain map with a red square. The main panel shows the bathymetry of the smaller model domain. The arrow marks the location of the river. The larger dots mark the stations where water samples (red) and mussel samples (green) were collected. The small black dots represent the Culture Units. Note that there are 4 Culture Units (on top of each other) occupying the middle of the water column, but this cannot be seen due to the perspective of this illustration.

and Hill, 1999) and Trinity Bay, Newfoundland (Thompson, 1984). The application of the model encompassed five modelling analyses, which we outline below.

2.2.1. Analysis 1 - Comparison against physical data

Using default parameters (Table 1), we ran the model to simulate two months (output at 15 min intervals) during a time of the year concurrent with our data of currents, temperature and salinity (see Section 2.6.1). Only the hydrodynamic module was used for this run.

2.2.2. Analysis 2 - Comparison against biochemical and mussel physiology data

We ran the model to produce a one-year simulation (output at daily intervals) to compare model output against water samples collected from 1988 to 1992 for analysis of nutrients, chlorophyll, oxygen and particulate organic matter (see Section 2.6.2) and against published rates of mussel physiology (Thompson, 1984; Cranford and Hill, 1999). We used default parameters (Table 1) and a mussel standing stock consistent with the stock reared at the time of collection of water samples (see Section 2.3).

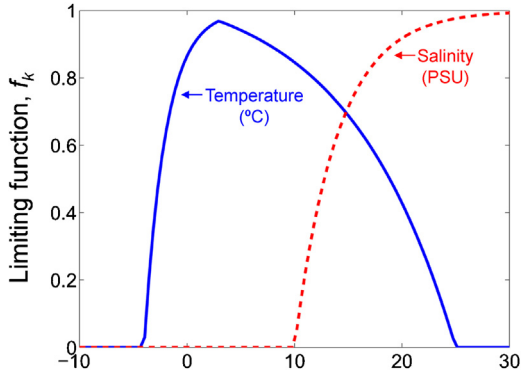

Fig. 2. Limiting functions for temperature (Eq. 6) and salinity (Eq. 7). Note that model equations are located in the online supplemental material.

2.2.3. Analysis 3 - Comparison against mussel size-classes

We ran the model to produce a one-year simulation (output at daily intervals) to compare model output against the size-distributions of mussels collected in 2001 (see section 2.6.3). Note that, while all mussels in a Culture Unit are identical (same size), it is possible to create a size distribution by inserting many Culture Units (each of different size) in a single grid cell.

We used default parameters (Table 1) and a mussel standing stock consistent with the stock reared during 2001. However, in the location where mussel samples were collected, we inserted 33 Culture Units, each initialized with a different initial biomass (i.e. initial size) so that the ensemble of Culture Units in that location would mimic the size-distribution of the mussel samples. At the end of the simulation, the size of all the mussels from all the Culture Units in that location were binned into size-classes to evaluate the resulting size-distribution after the one-year simulation.

2.2.4. Analysis 4 - Determination of production carrying capacity

In this study we evaluated the production carrying capacity, defined as the "optimized level of production" of aquacultured bivalves (McKindsey et al., 2006).

We ran 7 one-year simulations using the high resolution grid, and using all the default parameters from Table 1 (except Harvesting rate, $\lambda^{Harv} = 0\,d^{-1}$, see below). We ran each simulation with a different initial mussel density, ranging from 3 to 200 gdw m^{-3}. In this analysis we did not use the continuous harvesting scheme used in the previous analyses. Instead, for each simulation we estimated the harvest yield (tons), which was defined as the total mussel biomass at the end of the simulation minus the total biomass at the beginning of the simulation. The production carrying capacity was

determined as the smallest initial mussel density that produced the highest harvest yield.

2.2.5. Analysis 5 - Effect of natural mortality on the determination of production carrying capacity

We evaluated the effect that the natural mortality of bivalves has on the estimation of the production carrying capacity by estimating carrying capacity (using the procedure described above) at natural mortalities of 0, 0.0001, 0.0005 and 0.001 d^{-1}. In total we ran 28 one-year simulations to estimate the harvest yield as a function of initial mussel density and mussel natural mortality.

2.3. Study site

Ship Harbour is a long (10 km) and narrow estuarine fjord, with a deeper inner basin with maximum depth of 27 m, and a shallow sill with an approximate depth of 7 m. Mean tides are 1.4 m and spring tides are 2.0 m (Gregory et al., 1993). At the seaward boundary, Ship Harbour is open to the North Atlantic. The dominant source of fresh water is the Ship Harbour River (Fig. 3), discharging an annual average of 18 $m^3 s^{-1}$ (Gregory et al., 1993), and driving an estuarine circulation. There is a continuous supply of silicate via the river, and of phosphate via the estuarine circulation (Strain, 2002). Therefore, nitrate supplied from shelf waters during the winter controls most of the variability of chlorophyll and is the most important source of nitrogen driving new production in the spring bloom (Strain, 2002).

Ship Harbour has one of the largest mussel farms in Nova Scotia (Aquaprime Mussel Ranch Ltd.). Blue mussels (*Mytilus edulis* and *M. trossolus*) are grown in mesh socks suspended from long-lines (Sénéchal et al., 2008). Juvenile mussels are seeded at an approximate size of 8 mm (i.e. $B_k = 0.016$ mmol N ind^{-1}, see Table 1), and they are harvested 3 years later at a approximate size of 75 mm or 10 mmol N ind^{-1} (John Stairs, pers comm.). At the time of collection of the water samples used in this study (1988–1992), the farm contained about 225 tons of mussels (wet weight with shell; Strain, 2002), and at the time of collection of the mussel size-distribution samples (2001) the farm had about 1000 tons of mussels (Ibarra, 2003).

2.3.1. Model grids and grid nesting

We created a high resolution grid representing Ship Harbour (Fig. 3) which had 100 m × 100 m grid cells and 10 sigma layers. One-year simulations using the high resolution grid required about 1 day to run on 4 CPUs on our computer system (Linux cluster with 2.8 GHz Opteron processors). In the grid, the seaward open boundary was forced with output from a large meso-scale ROMS model for the North-East North American shelf (Fig. 3), which has been described in detail in Fennel et al. (2008).

2.4. Forcing

Wind speed, air temperature, air pressure, relative humidity and rainfall rate from archive records (2004–2005) were obtained from the meteorological station in Shearwater Airport (http://www.meds-sdmm.dfo-mpo.gc.ca/isdm-gdsi/azmp-pmza/met/plot-graph-eng.asp?a=30), which is approximately 50 km from the study site. Short wave radiation was obtained from a Satlantic Land/Ocean Biogeochemical Observatory (LOBO; http://lobo.satlantic.com), about 55 km from the study site. The LOBO buoy was not operational during the time period of the simulations, therefore we shifted the LOBO data in time by subtracting 5 years from the time stamps. We assumed that the dynamics in Ship Harbour are mainly driven by the seasonal signal of short wave radiation, and that daily variability is not as important.

The open boundary at the seaward end of Ship Harbour was forced with output from the WebTide tidal prediction model (Department of Fisheries and Oceans, Canada; http://www2.mar.dfo-mpo.gc.ca/science/ocean/coastal_hydrodynamics/WebTide/webtide.html). Also, the concentrations of all planktonic ecosystem variables entering the open boundary were forced using output from the meso-scale ROMS model described above.

Fresh water entering Ship Harbour through the river was simulated using a synthetic time-series created using data from Gregory et al. (1993). The concentration of the planktonic ecosystem tracers in the river's water was set to resemble a seasonal pattern (e.g. Dowd, 2005).

2.5. Initial conditions

All physical and planktonic ecosystem variables were initialized with constant values over the entire domain. Simulations began after a six-month model spin-up to allow physical and planktonic ecosystem variables to reach a distribution representative of the model dynamics. However, the individual-based variables (i.e. mussel soma, gonad and number of individuals) were reset at the beginning of the simulation, to evaluate their evolution from a uniform condition.

2.6. Data collection and analysis

2.6.1. Physical data

Temperature, salinity and current velocity were measured every 10 min from September 19 to October 15 of 2001 using a CTD/current meter (2D-ACM, Falmouth Scientific, Inc.) moored at 4.5 m from the bottom (Fig. 3). Instrument deployment did not coincide with the period for which boundary forcing was available. That is, our model results correspond to a different year from the year when physical data were collected. Therefore, we restricted data/model comparison to seasonal means and did not attempt to explain short term variability.

2.6.2. Biological and chemical samples

Biological and chemical data were obtained from the BioChem database (DFO, 2005) and correspond to water samples collected in Ship Harbour (Fig. 3) from 1988 to 1992. Data have been published elsewhere (Keizer et al., 1996; Strain, 2002); here we present only a brief description of their sample analysis. Ammonia and nitrates (i.e. nitrate + nitrite) were measured with autoanalyzer techniques (Strain, 2002), oxygen concentration was determined using a polarographic oxygen electrode (1991 survey) and Winkler titrations (1992 survey). Chlorophyll concentrations were determined using extracted fluorometry (Strickland and Parsons, 1968). Suspended particulate matter (SPM) was estimated using preweighed filters and gravimetric analysis (Winneberger et al., 1963).

2.6.3. Size-distribution of mussels

Mussels in Ship Harbour were sampled in September 2001 (Ibarra, 2003). At the time of collection, mussels from each of the three year classes were sampled from the lease shown in Fig. 3. The length of individual mussels was measured and size-distributions for each year-class were calculated. See Appendix A for the equation to convert from mussel length into biomass.

3. Results and discussion

In the first five subsections below, we combined the results and discussion of each of five self-contained analyses. For clarity, results are presented in past tense, while discussions are written in present tense.

3.1. Comparison against physical data (Analysis 1)

We compared modelling results of temperature, salinity and current speed against observations recorded with a CTD/current meter deployed in Ship Harbour in 2001 (Fig. 4). Observed average current speeds in the East–West and North–South directions were 0.03 m s^{-1} and 0.002 m s^{-1} higher than the modelled average speeds, respectively. Observed average temperature was the same as the model (15.4 °C), but the observed average salinity was 0.1 PSU lower than the model. Considering that the model simulation corresponded to a different year from the observations (but same dates), the relatively small discrepancies between model and observations indicate that the model is reproducing the main hydrodynamic features of Ship Harbour. However, it is important to be aware that comparisons of histogram distributions (e.g. Fig. 4) is not a very robust validation method because it cannot resolve differences in phase or in vertical structure.

3.2. Comparison against biochemical and mussel physiology data (Analysis 2)

3.2.1. Planktonic ecosystem

Water-column planktonic ecosystem variables showed large spatial variability through Ship Harbour, as well as pronounced seasonal variability (Fig. 5). The spring bloom caused the largest concentrations of phytoplankton nitrogen, chlorophyll, oxygen and large detritus; while the lowest concentrations of phytoplankton, chlorophyll, zooplankton and small detritus were seen in winter. Concentrations of nitrate and large detritus were lowest in the summer.

We compared observations from water samples collected from 1988 to 1992 against a one-year model simulation (Fig. 6). Modelled phytoplankton nitrogen and chlorophyll concentrations showed seasonal variability with a very distinguishable spring bloom (peak of 4.2 mmol N m^{-3} or 17 mg Chl m^{-3}, see Fig. 6) and a less distinguishable fall bloom (peak of 2 mmol N m^{-3} or 13 mg Chl m^{-3}). However the largest modelled concentrations occurred during late December (5.2 mmol N m^{-3} or 23 mg Chl m^{-3}). Both, phytoplankton nitrogen and chlorophyll, also showed periodic variability with a period of about 15 days, that is likely due to the spring-neap tidal cycle. Modelled chlorophyll is within the range of observations from water samples. However, the model did not reproduce very high peaks of chlorophyll seen sporadically during the summer. These peaks may be attributed to vertical migrations of phytoplankton (e.g. Hall and Paerl, 2011), resuspension of microalgae and detritus of macroalgae during wind events (e.g. MacIntyre and Cullen, 1996; Koh et al., 2006), or enhanced productivity associated with resuspension of sediments (e.g. Chen et al., 2010). Modelled chlorophyll also overestimated the observed concentration during late December to mid March. We speculate that the overestimation is because the model did not account for ice formation during winter months, which drastically reduces light penetration (Pegau and Zaneveld, 2000).

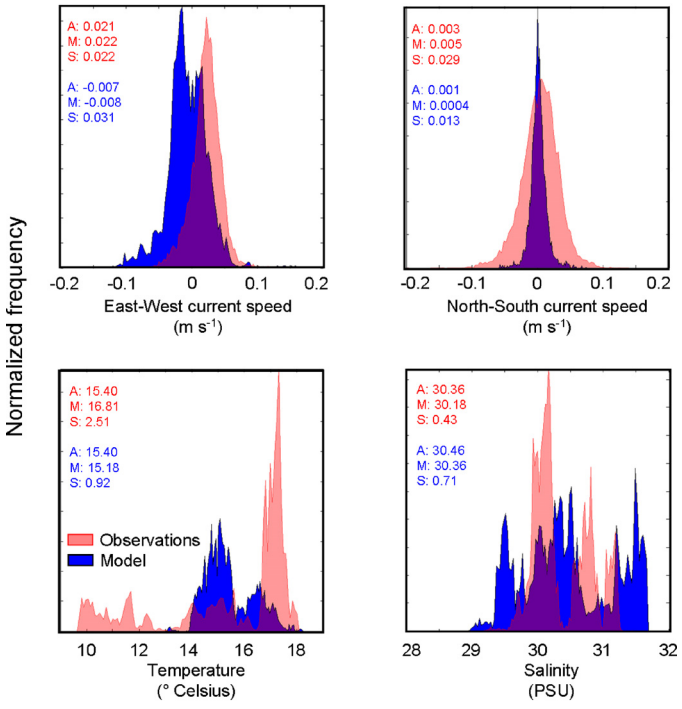

Fig. 4. Comparison of hydrodynamic observations (red) against model results (blue). Histograms show the distribution of current speeds, temperature and salinity, recorded every 10 min at 4.5 m above the bottom, from September 19 to October 15 (n = 3605). Observations were made in 2001 (see location in Fig. 3), however model results correspond to the same period in 2005, because the 2001 forcing was not available. Numbers are averages (A), medians (M) and standard deviations (S).

Modelled zooplankton was highest during late spring (4 mmol N m^{-3}) and lowest during the winter (0.5 mmol N m^{-3}). However, unlike phytoplankton, zooplankton concentrations remained relatively high during summer months. The zooplankton time series also showed an oscillation of approximately 15 days, likely due to the spring-neap tidal cycle.

Oxygen concentrations from both, water samples and model, showed highest concentrations when the water was coldest and lowest concentration when water was warmest, in accordance with oxygen solubility properties of seawater (Garcia and Gordon, 1992). However, the observations showed a much larger variability with depth, where lower concentrations were seen in deeper waters. At times, oxygen concentration in deeper waters was as low as 20 mmol O_2 m^{-3}; close to the hypoxic threshold of 17.5 mmol O_2 m^{-3} (Wang and Widdows, 1993). The model did not reproduce the low oxygen concentration observed in deeper waters. This implies that there are oxygen sinks in Ship Harbour that are not accounted for by the model. Also, our model immediately remineralizes organic matter reaching the bottom, while in nature remineralization is spread out over seasons (Strain, 2002).

In both model and observations, ammonia was low in the winter (approximately 1 mmol N m^{-3}) and increased during the spring and summer as the water-column stratified (approximately 20 mmol N m^{-3} for the observations and 5 mmol N m^{-3} for the model). However the increase in ammonia concentration was much more pronounced in the observations (up to 48 mmol N m^{-3}) than in the model (up to 9 mmol N m^{-3}). Again, this suggests that there is a source of organic matter not accounted for in the model. Strain (2002) were also puzzled by the high ammonia concentrations in Ship Harbour, which they could not explain by the presence of mussels alone.

Nitrate concentration in the model and the observations were high during the winter and late fall (up to 8 mmol N m^{-3}) and very low during the summer (0 to 0.25 mmol N m^{-3}). Strain (2002) analysed nitrate-salinity relationships and concluded that nitrate in Ship Harbour likely comes from shelf water when the water column is mixed. Our model results are consistent with Strain's (2002) description of the nitrate dynamics in Ship Harbour.

The concentration of both small and large detritus follow similar patterns, with highest concentrations in late spring (1.5 and 3.2 mmol N m^{-3} for large and small detritus, respectively), intermediate concentrations in the summer and early fall, and lowest concentrations in the winter (0.1 and 0.9 mmol N m^{-3} for large and small detritus, respectively). Throughout the year, the concentration of small detritus was about double the concentration of large detritus. The modelled concentration of

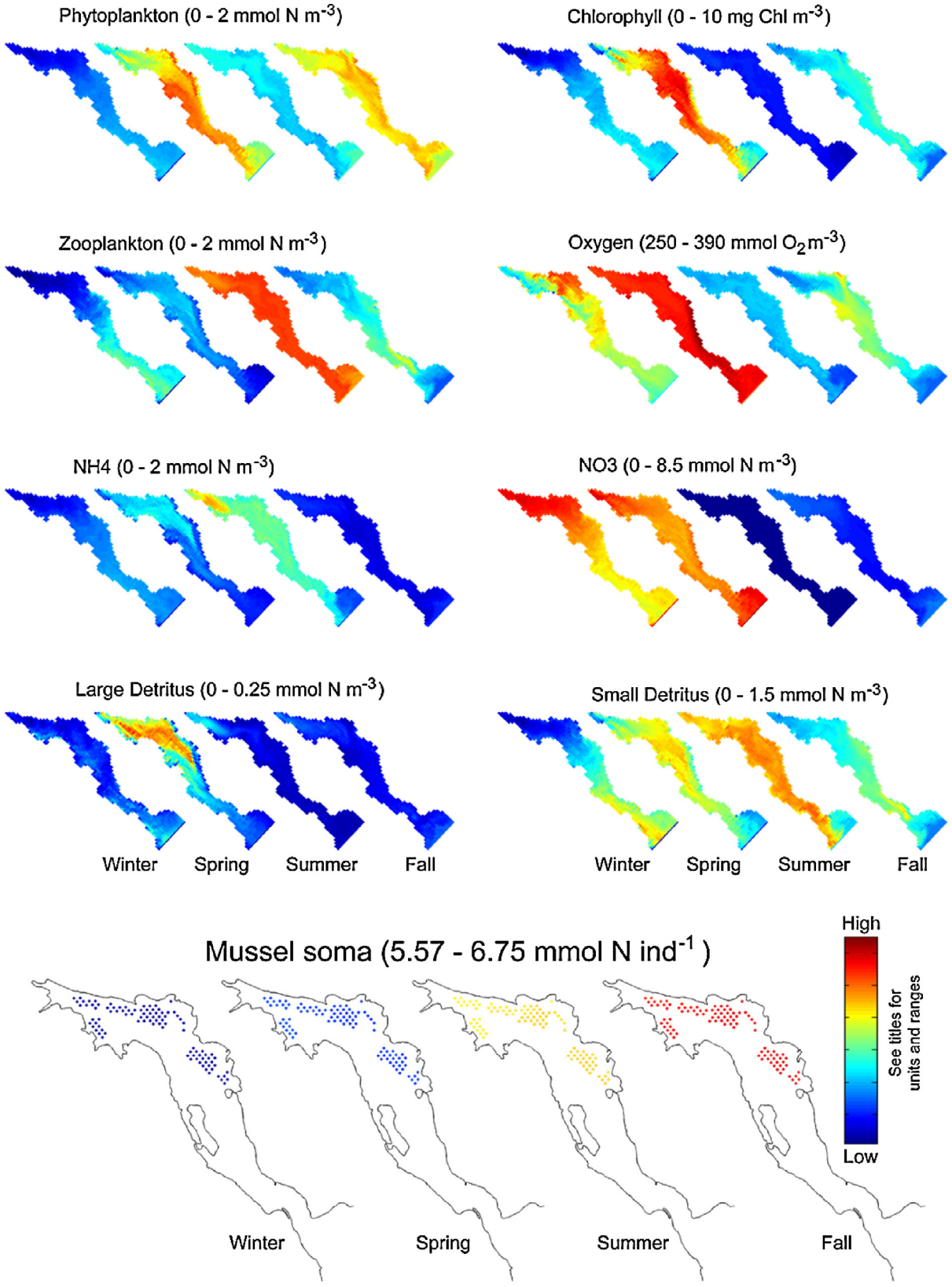

Fig. 5. Four snapshots (winter, spring, summer and fall) of all Eulerian planktonic ecosystem state variables (coloured maps) and of the individual-based mussel soma (dotted maps) for Ship Harbour. All maps are top-views of the middle of the water column. The range and units of the colour-coding is the same among maps of the same variable, but different among variables (see parenthesis).

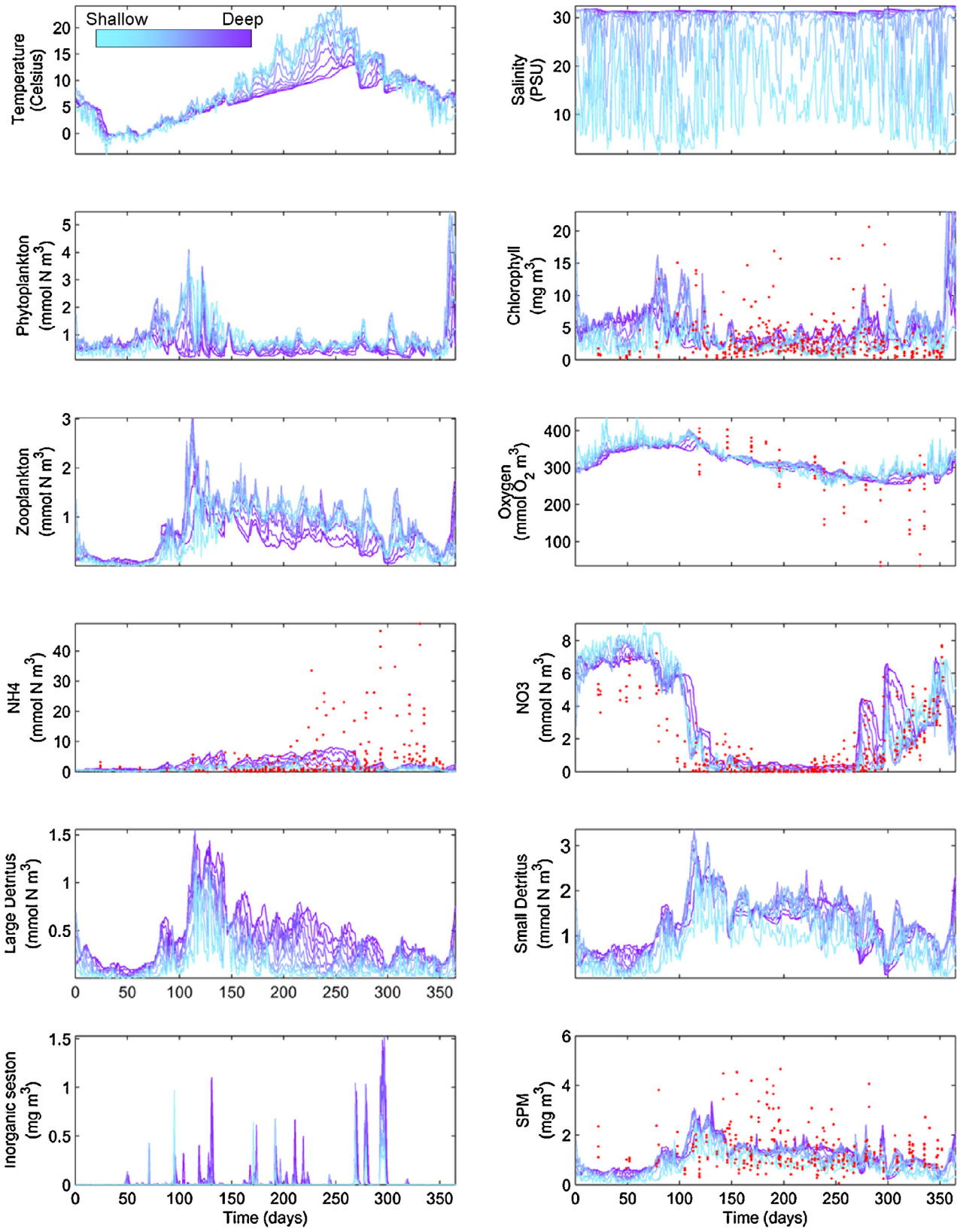

Fig. 6. Comparison of biological and chemical observations from water samples (red dots) against model time-series from the same location (blue/purple lines; see collection location in Fig. 3. Lighter blue lines correspond to shallower layers while darker purple lines correspond to deeper layers. Water samples were collected between 1988 and 1992 but model simulation is for 2005, because earlier forcing was not available.

suspended inorganic particles showed sporadic spikes (maximum of 1.5 mg m^{-3}), consistent with resuspension of sediments during strong wind events. The concentration of suspended particulate matter (SPM; i.e. large detritus + small detritus + inorganic sediments + phytoplankton + zooplankton) predicted by the model was roughly within the range observed from the water samples. However the model could not reproduce some of the large spikes observed in the data. This is probably because the model did not account for resuspension of material from the mussel socks, which is likely greater than resuspension at the bottom, because socks are closer to the surface where they can experience higher current speeds.

In this study we only give an overview of environmental changes in the water column because the effect of aquacultured bivalves on the environment in Ship Harbour was studied in detail elsewhere (Ibarra, 2011).

3.2.2. Mussel physiology

We compared modelling results from the individual-based SHELL-E model against published physiological rates from different parts of Atlantic Canada (Thompson, 1984; Cranford and Hill, 1999). The modelled number of individuals in all Culture Units decreased exponentially (Fig. 7; from 2–7 × 10^4 ind, to 1–4 × 10^4 ind) due to natural mortality and harvesting. Modelled soma (i.e. structural biomass of mussels) increased throughout the year (from 6.3 to approximately 6.8 mmol N ind^{-1}), however it increased more slowly after May. Modelled mussels at different locations grew at different rates. Although all mussels started the simulation with the same biomass, at the end of the one-year simulation there were differences in soma biomass of up to 0.5 mmol N ind^{-1}, with higher values in mussels in surface layers (Fig. 5). In model runs with higher initial density, this difference was 1.5 mmol N ind^{-1} (data not shown), including some mussels that did not gain any biomass during the one-year model simulation. Mussels in the surface layers appeared to grow faster than the rest, which is consistent with observation (J. Stairs, pers. comm.).

The shell length of modelled mussels was estimated diagnostically using an empirical relationship for Ship Harbour (Ibarra, 2003; see Appendix A). Because it was calculated from biomass, it followed the same pattern as the soma, where slower growth occurred during the winter months, and faster growth during the spring, particularly in mussels in surface layers.

The most notable pattern of the gonad state was the three spawning events. However, Guyondet et al. (2010) stated that it is common for mussels of the region to spawn 2 times per year. The discrepancy in numbers of spawning events per year may be attributed to the fact that mussels in our model spawn simply by reaching a soma/gonad threshold, while real mussels are known to spawn not only when their gonads are full, but also when presented with a temperature cue (Gosling, 2003), which was not programmed in the modelled mussels. Like the soma, mussel gonads grew all year round (except during spawning events); however gonad growth was slower during the winter. Also, the gonads of mussels close to the surface grew faster and therefore, mussels close to the surface were usually the first to spawn. The total biomass of modelled mussels showed a large variability during the one-year simulation, mainly because of the spawning events, but also because of the spatial variability observed in soma growth among the modelled mussels.

Clearance rates varied throughout the one-year simulation showing both low and high frequency variations. Most of the modelled clearance rates were between 0.5 and 2.8 L gdw^{-1} h^{-1} (i.e. 0.002 and 0.012 m^3 mmol N^{-1} d^{-1}), however there are some short moments where clearance rates in the surface layers were completely shut down because of low salinity. Also, there were some short peaks when clearance rates almost reached 4 L gdw^{-1} h^{-1} (i.e. 0.017 m^3 mmol N^{-1} d^{-1}). One of the advantages of the SHELL-E model is its ability to separately track the different limitations modulating clearance rates. Therefore we can evaluate which environmental factor had the largest impact during different times of the year.

Temperature played a large role in limiting modelled filtration during months with hot water temperature, particularly in surface layers. However, in this study, the limitation of filtration by temperature was regulated by parameters that we chose from a study from Newfoundland (Thompson, 1984). These parameters imposed a reduction in the modelled filtration rate of up to 80% in the summer. We cannot verify if this temperature effect on filtration indeed occurred. However, based on anecdotal information from mussel farmers, we think that mussels in Eastern Canada are stressed during the weeks of hottest temperatures. This limitation due to high temperature may be restricted to populations of mussels acclimated to cold water, since some population of mussels in Italy have been shown to exhibit normal filtration rates at temperatures above 25 °C (Schulte, 1975).

Food limitation also played an important role modulating modelled clearance rates during most of the year (except during hot months, where temperature was the main limiting factor). Food limitation showed high frequency variations due to the tides (lowest during slack tides) and was responsible for the high frequency variability in clearance rates.

Oxygen did not play an important role in our "standard" simulation, however in other model runs with high mussel densities, mussels depleted oxygen enough to cause a limitation as low as 0.4 of the maximum rate (data not shown).

Salinity only played a small role, where it limited filtration only for short periods of time and only in surface layers. However, it is important to emphasise that the limitation of filtration by salinity was mediated through parameters we chose from a study assessing the impact of salinity on shell growth (Almada-Villela, 1984). We assumed that a decrease in shell growth reflects a decrease in filtration, but this may not be the case. The sporadic, yet pronounced, decreases in filtration due to low salinity in our modelled results (Fig. 7) are the results of our choice of parameters and we do not have any way to verify if this phenomenon indeed happens in Ship Harbour. However, this can be seen as a new hypothesis that needs field data to be tested, with results being used to improve the parameterization. Overall, the effect of salinity on our modelled results was minimal and limited only to the mussels closest to the surface.

Modelled assimilation rates were highest during blooms in the spring and late fall (approximately 40 mg gdw^{-1} d^{-1} or 0.6 mmol N ind^{-1} d^{-1}) and remained about 8 mg gdw^{-1} d^{-1} (or 0.1 mmol N ind^{-1} d^{-1}) for the rest of the year (see Appendix A for conversions). The variability in the assimilation rate was within the range reported by Cranford and Hill (1999), however they observed the highest rates only during the fall. Modelled excretion rates were also highest during blooms in the spring and late fall (approximately 20 μg N gdw^{-1} h^{-1} or 0.06 mmol N ind^{-1} d^{-1}) and remained about 3 μg N gdw^{-1} h^{-1} (or 0.01 mmol N ind^{-1} d^{-1}) for the rest of the year. The variability in excretion rates was within the range reported by Thompson (1984), however he observed the highest rates only during early fall, when water temperature was warmest. Time-series of both, assimilation and excretion rates (Fig. 7) showed variability consistent with the variability in the time-series in phytoplankton biomass (Fig. 6).

Egestion rates were highest during the spring bloom (up to 40 mg gdw^{-1} d^{-1} or 0.4 mmol N ind^{-1} d^{-1}); however they remained relatively high during the summer. Unlike the rates of assimilation and excretion, that closely resemble the time-series of phytoplankton, the rate of egestion depended more strongly

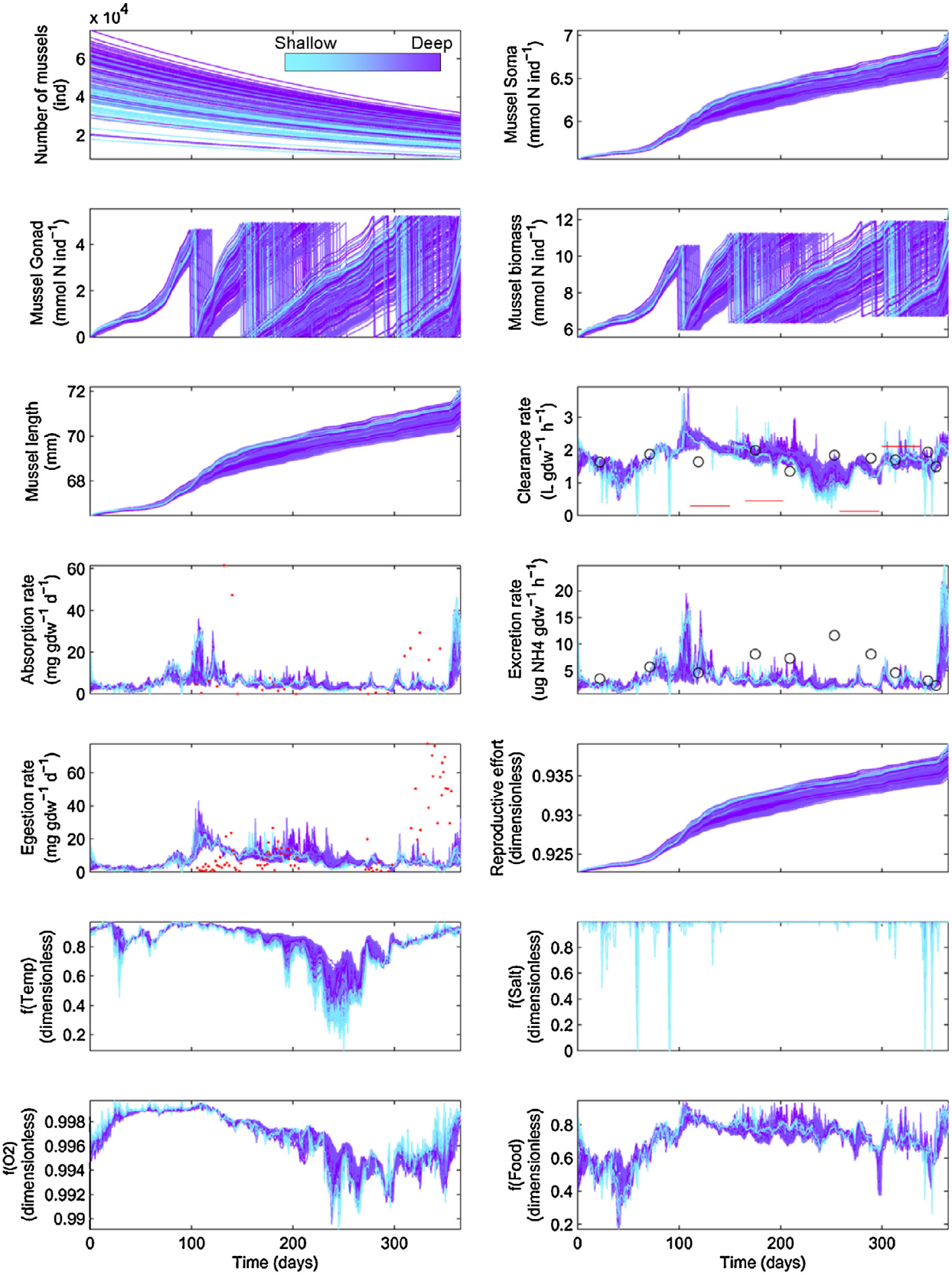

Fig. 7. Comparison of results from the individual-based shellfish ecophysiology (SHELL-E) model (blue/purple time-series) against published physiological rates (black circles = Thompson 1984; red dots or lines = Cranford and Hill, 1999). Lighter blue lines correspond to shallower layers while darker purple lines correspond to deeper layers.

on the local concentration of detritus and zooplankton. This is because mussels have lower assimilation efficiencies for zooplankton and detritus, compared to the assimilation efficiency for phytoplankton. Therefore, a large portion of the filtered zooplankton and detritus ends up egested as undigested faeces. Simulated egestion rates were within the range of rates measured in the field (Cranford and Hill, 1999). However, observed rates were highest in the fall when water temperature was the warmest.

The time series of reproductive effort resembled the series of soma and length, because both, soma and reproductive effort, are calculated diagnostically as a function the soma biomass. All mussels in the simulation were initialized to have the same initial size of 63 mm (1 gdw or 5.56 mmol N), which is the size of a "standard" adult mussel. This facilitates comparisons with physiological rates in the literature; however, because all mussels in the simulation were adults, the modelled reproductive effort shows only a slight increase (from 0.92 to 0.94) over the one-year simulation.

Note that, because of the lack of physiological experiments conducted on the same species and under the same environmental conditions as our model application, we were forced to use less appropriate parameters adapted from the available literature. Sarà et al. (2013) identified this is a common bottleneck in many models, and provided insight on how to circumvent this problem.

3.3. Comparison against mussel size-classes (Analysis 3)

We compared size-frequency distribution from mussels collected in 2001 against predicted size-distributions after a one-year model simulation (Fig. 8). Comparing the modes of each distribution, we saw that mussels of the 2000 year-class grew in the model from 40 to 50 mm during the one-year simulation (i.e. from panel A to panel D in Fig. 8). Similarly, mussels of the 1999 year-class grew in the model from 60 to 65 mm (from panel B to panel E), and mussels of the 1998 year-class grew in the model from 65 to 70 mm (from panel C to panel F). Comparing sizes of mussels of the same age—that is, panel B with D, and panel C with E—we found that modelled growth of younger mussels was somewhat slower than the inferred from the measured differences between age classes (i.e. 10 mm year^{-1} or from A to D, instead of 20 mm year^{-1} or from A to B), while the modelled growth of older mussels (5 mm yr^{-1} or from B to E) was the same as the measured difference (from B to C). At the end of the simulation, the modelled variability in size of the 2000 and 1999 year-classes (panels D and E) was smaller than the observed variability of the measured counterparts at the beginning of the simulation (panels B and C). This is partially because the model does not account for the recruitment of seedlings from the spawning events, which accounted for the smallest size-classes in the initial (i.e. measured) distributions. Additionally, in this study, natural mortality (λ^{Nat}) was assumed to be independent of size. While the effect of size on natural mortality of mussels is largely unknown, it has been shown that the natural mortality of clams varies with size (Andresen et al., 2013). The imposed constant natural mortality rate may be responsible for some of the discrepancies between the observed and modeled mussel size distributions (Fig. 8), where the model tended to overestimate the abundance of mussels smaller than the median.

Considering that the model was forced with atmospheric and boundary conditions from 2005, while mussels were sampled in 2001, we concluded that the model predicts mussel growth satisfactorily.

3.4. Determination of production carrying capacity (Analysis 4)

We estimated the production carrying capacity for farmed mussels in Ship Harbour using multiple one-year simulations of the hybrid model to determine the relationship of harvested yield as

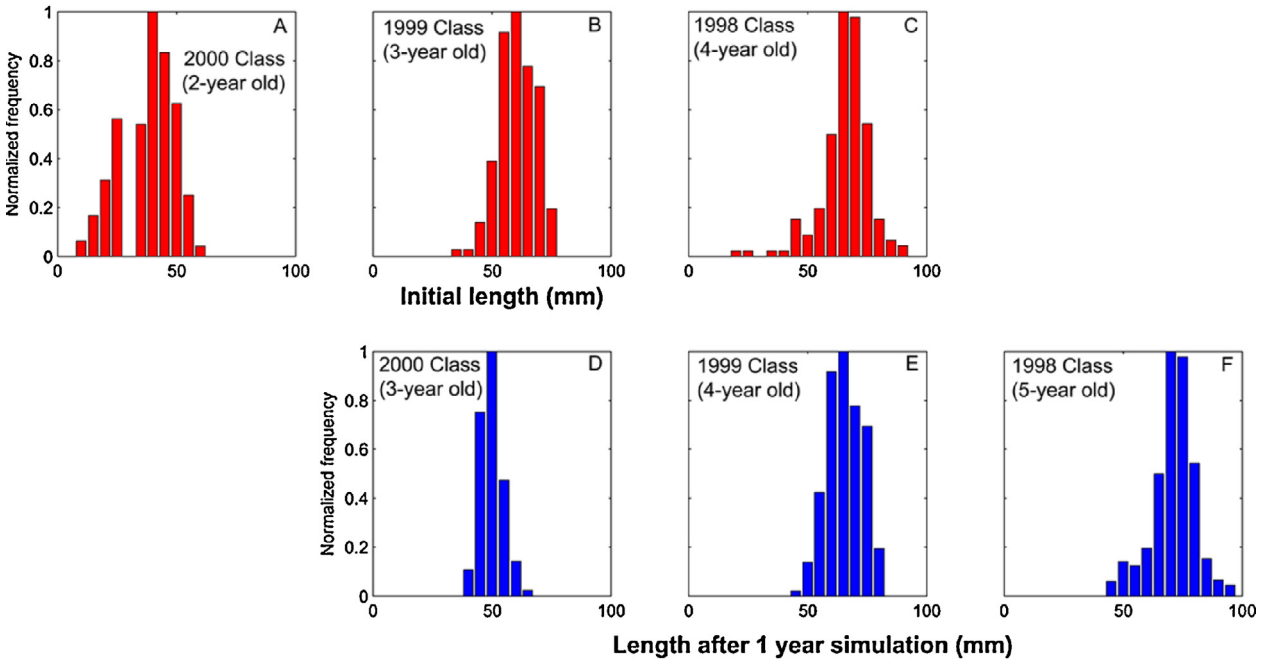

Fig. 8. Measured histograms of size-distributions of mussels collected in Ship Harbour in 2001 from three year-classes (panels A, B and C; in red). Note the seeding is done with 1-year old juvenile mussels purchased from a different site. Therefore, for clarity, we included in parentheses the age of mussels at the time of collection. These measured size-distributions were used to initialize the biomass of multiple Culture Units that were inserted at a single location corresponding to the location where the mussels were collected. After a one-year model simulation, the resulting size-distribution from the ensemble of Culture Units (panels D, E and F; in blue) can be compared against mussels of the same age from the initial distributions (i.e. compare D against B, and E against C).

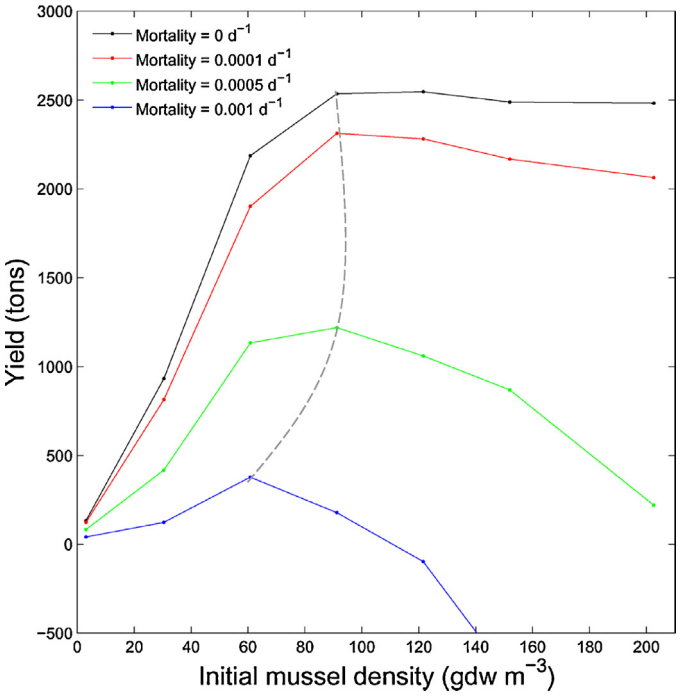

Fig. 9. Estimation of production carrying capacity for a mussel farm in Ship Harbour. Each density-yield curve was generated using multiple one-year simulations of our hybrid model, and each curve depicts the relationship between initial seeding density and harvested yield under one of four scenarios with different natural mortalities. For each curve, the production carrying capacity is estimated as the point of the curve with the maximum yield. The grey dashed line connects the maximum yields of all four mortality scenarios.

a function of initial seeding density[1] and natural mortality (Fig. 9). For any given natural mortality, at low initial seeding densities, the harvested yield increased substantially with small increases in initial density. However at intermediate seeding densities, mussels became food limited, thus small increases in initial density translated into minimal or null increases in yield. Finally, at high initial seeding densities, food limitation was so strong that mussels in the centre of the lease did not get enough food to offset their catabolic metabolism (Eq. 2 in online supplemental material) and natural mortality (Eq. 17 in online supplemental material), so the Culture Units started to lose weight. Therefore, the harvested yield at high seeding densities actually decreased compared to the yield estimated at intermediate seeding densities. The production carrying capacity of the system is the optimized level of production (McKindsey et al., 2006), which is usually reached when seeding at an intermediate seeding density. Farmers seeding mussels at a lower density than the optimal density are underutilizing their resources, while farmers seeding above the optimal seeding density are overexploiting their resources, wasting seeding effort, and ultimately not harvesting as much as with a smaller initial density.

Note that, at low initial densities, the resulting yield increased exponentially with initial density (Fig. 9). That is, at low initial densities, a doubling of the initial density (e.g. from 20 to 40 gdw m^{-3}, at mortality = 0 d^{-1}) resulted in more than a doubling of the resulting yield (e.g. from 600 to 1400 tons). We speculate that this may occur because mussels may act as biocapacitors, which are "charged" with nitrogen during times of abundant food (e.g. spring bloom) and then slow-release their charge throughout the year, effectively subsidizing primary production during times of low nutrients (i.e. during the summer). In other words, mussels may help to retain nitrogen in the system, thus increasing nitrogen recycling. As stated in previous work (Grangeré et al., 2010), bivalve aquaculture models must have two-way coupling between bivalve physiology and lower-trophic dynamics, to be able to resolve these feedbacks.

For Ship Harbour, we estimate that the production carrying capacity should be achieved at mussel seeding densities of approximately 60 gdw m^{-3} (for a natural mortality of 0.001 d^{-1}), yielding a harvest of about 400 tons of mussels per year. The current seeding density in Ship Harbour is about 33 gdw m^{-3} (Ibarra, 2003) suggesting that aquaculture activities in Ship Harbour have not reached their production carrying capacity. However, we do not advise to increase their seeding densities on the basis of this prediction alone, because of uncertainties associated with our estimation of the natural mortality rate of mussels (see section below). This parameter has to be accurately estimated before the model can provide a more reliable estimate of the production carrying capacity for Ship Harbour.

3.5. *Effect of natural mortality on the determination of carrying capacity (Analysis 5)*

Our results show that natural mortality played an important role in the estimation of harvest yield, where higher mortalities translated into lower yields. However, the more interesting result is that the shape of the density-yield curves changed with increasing mortality. That is, the harvest yield at high initial densities decreased very rapidly in scenarios with high mortality; sometimes to the point where the harvests are less than the initial seeding (i.e. negative yield). The main implication of this change in shape of the density-yield curves is that the maximum yield (i.e. production carrying capacity) shifts towards smaller initial densities at higher natural mortalities. In our lower-mortality simulations, a five-fold increase in natural mortality (from 0.0001 to 0.0005 d^{-1}) did not change the estimated maximum yield (90 gdw m^{-3}). However in our higher mortality simulations, a doubling of the natural mortality (from 0.0005 to 0.001 d^{-1}) resulted in a 33% decrease in yield (from 90 to 60 gdw m^{-3}). Our results emphasize the importance of considering natural mortality when attempting to estimate the production carrying capacity of a farm. Some bivalve-environment models designed to estimate carrying capacity do not explicitly account for bivalve mortality (e.g. Incze et al., 1981; Sarà and Mazzola, 2004; Grant et al., 2007; Filgueira et al., 2010). Other carrying capacity models do take bivalve mortality into consideration (e.g. Dame and Prins, 1998; Duarte et al., 2003; Guyondet et al., 2010), but these studies do not investigate the effect of natural mortality on the estimated production carrying capacity. However, there are a few studies investigating the effect of natural mortality on bivalve standing stock (e.g. Bald et al., 2009).

3.6. *Comparison of model results against data*

Data-model comparisons showed that our model predicts planktonic ecosystem variables and bivalve physiology variables within ranges observed in the field (Fig. 6 and Fig. 7). However, due to restricted availability of forcing, our model results correspond to a different time from the time of collection of the observations. Also, some observations (from Cranford and Hill, 1999 and Thompson, 1984) were collected from different embayments than the modelled study site. This lack of concomitance limits the ability of the data to reject the model (Franks, 2009). That is, it is difficult to separate how much of the differences between the model results and observations are due to spatial and temporal differences, and how much is due to inadequacies of the model, or errors in our assumptions. However, even with these limited abilities, the

[1] Note that the mussel densities (units: mmol N m^{-3}) reported in this study reflect the bivalve biomass divided by the volume of the mussel lease. Other studies used as a reference the volume of the entire inner basin of the fjord (e.g. Strain, 2002).

available data provided a frame of reference that allowed us to constrain the model, and to evaluate the overall range of the modelled output.

3.7. Advantages of hybrid (Eulerian/IBM) ecosystem models

The main disadvantage of traditional Eulerian models is that they run too slowly when tasked with representing many state variables in a high-resolution 3-D grid. Therefore, Eulerian models designed to represent complex bivalve physiology with many state variables are often limited to use domains with fewer grid cells (i.e. box models or 2-D grids) and/or to neglect planktonic primary productivity processes. Similarly, Eulerian models using 3-D high-resolution grids are often limited to use simple bivalve physiology models (i.e. low physiological resolution). In our hybrid model, we decoupled the bivalves from the Eulerian grid-based framework, allowing us to represent complex bivalve physiology in a 3-D high-resolution domain while maintaining two-way coupling between bivalves and planktonic primary productivity processes.

As mentioned above, early models were able to represent complex bivalve physiology (at reasonable model speeds) by neglecting local primary production (e.g. Incze et al., 1981; Bacher et al., 2003). That is, these models implemented a one-way coupling scheme between plankton and bivalves, where the local concentration of phytoplankton only depended on the balance between material entering the model domain (via forcing through an open boundary) and material filtered by the bivalves. These models cannot resolve feedbacks between bivalve physiology and phytoplankton dynamics, which are thought to be important in applications where the residence time of water within the domain is comparable to the doubling time of phytoplankton (Pilditch et al., 2001). The application of bivalve-environment models neglecting primary production should be restricted to lease-scale applications (Ibarra, 2003).

Other bivalve-environment models do include primary productivity and two-way coupling with lower-trophic level process, but at the expense of spatial resolution. These are ecosystem box models, where an entire bay is represented with a single box (i.e. 0-D models; e.g. Dowd, 1997; Dame and Prins, 1998; Rosland et al., 2009) or with a few boxes (i.e. coarse 2-D models; e.g. Grant et al., 2007; Troost et al., 2010). These models assume that the contents of the box are completely mixed, thus bivalves have access to all the food within a box. In reality, food is usually not distributed homogeneously within a bay. Physical process such as solar heating of surface waters and freshwater runoff can produce water stratification, and biological process such as the filtration by bivalves can produce gradients in the distribution of phytoplankton (Ibarra, 2003; Grant et al., 2008). The differences between a fine-scale 3-D model and a coarse 2-D model was briefly studied by Guyondet et al. (2010). They compared results from their 3-D model for the Grande-Entrée lagoon (Iles-de-la-Madeleine, Québec, Canada) against results from a 2-D multiple-box model for the same region (Grant et al., 2007). The coarse 2-D model predicted a reduction in the concentration of phytoplankton of 15%, and a reduction of bivalve growth of 11%, as a result of a doubling in bivalve biomass. The fine-scale 3-D model predicted a 2.6% reduction in phytoplankton and a 3.5% reduction in bivalve growth as a result of the same doubling in bivalve biomass; however there were other differences between the two models apart from their spatial resolution. Spillman et al. (2008) also developed a fine-scale 3-D model and argued that—compared to coarse 1-D or 2-D models—their model predicted lower concentrations of food (and higher waste) in grid cells closest to their modeled bivalves; however, bay-averaged concentrations of food and nutrients remained relatively unaffected.

As we mentioned before, there are other advanced bivalve-environment models that coupled physical-biological and bivalve physiology models, and that are spatially resolved by using fine scale grids in 2-D (Duarte et al., 2003; Grant et al., 2008; Grangeré et al., 2010; Guyondet et al., 2010) and fine grids in 3-D (Spillman et al., 2008; Leon et al., 2011). All these are Eulerian or grid-based models and therefore their state variables must be defined in all grid cells within the model domain; hence, equations must be solved for each variable and for each grid cell. This is the main disadvantage of Eulerian models, where only a limited number of variables can be added (e.g. additional bivalve species, or size-classes, or physiological state variables) before the model slows down beyond practical limits. Therefore, Eulerian models with many grid cells (i.e. 3-D) may be limited to use simple physiological models, while Eulerian models using many bivalve physiological variables (e.g. *Soma*, *Gonad*, $f(Temp)$, $f(Salt)$, $f(Oxy)$, etc.) may be limited to use 2-D domains with fewer grid cells.

In our hybrid model, bivalves are represented using sparsely distributed particles. Adding particle-based variables also increases the length of time required to finish a simulation, however the increase in time depends on the number of particles, and not on the number of grid cells. Therefore, the Eulerian portion of the hybrid model can be 3-D and with many grid cells, while the IBM portion of the model can track many variables, without compromising the speed of the model (see Ibarra, 2011). The particle-based portion of our hybrid model tracks 3 prognostic and 17 diagnostic variables (see Table 1). The prognostic variables (i.e. $Soma_k$, $Gonad_k$, n_k,) allow the hybrid model to represent complex physiological processes (e.g. spawning events), however these variables are not the best candidates for model testing (Franks, 2009) because they depend on the balance of many processes, thus the "right" outcome can be achieved with many parameter combinations. Franks (2009) suggests that diagnostic variables representing physiological rates (e.g. A_k, R_k, F_k, etc.) are much better suited for model testing because they depend on fewer parameters than the state variables, and because they are directly comparable against results from laboratory and field experiments. Our hybrid model tracks a large number of diagnostic variables (e.g. A_k, R_k, F_k, RE_k, $f_k(Temp)$, $f_k(Salt)$, $f_k(Oxy)$, etc.), many of them representing physiological rates, which increases the options to constrain and test the model. Additionally, many of the diagnostic variables tracked by our model are very valuable in site selection and farm management. For example, a map of $f_k(Temp)+f_k(Salt)+f_k(Oxy)$ can help a farmer select the location for a new lease. The ability of hybrid models to employ many particle-based variables makes them an ideal candidate to simulate ecosystems with multiple species and/or polyculture farms (e.g. Ibarra, 2011; Sarà et al., 2012), and to simulate scenarios with multiple size-classes in each grid cell (e.g. this study).

4. Conclusions

We developed a hybrid Eulerian/IBM modelling system capable of two-way coupling planktonic ecosystem and bivalve ecophysiology processes. The Eulerian part of the modelling system was used to represent grid-based processes such as phytoplankton photosynthesis, grazing by zooplankton, uptake of nutrients and mineralization of detritus; while the IBM part of the modelling system represented bivalve ecophysiological processes, e.g., filtration, assimilation, excretion, egestion and mortality. The simultaneous and combined simulation of these grid- and particle-based processes allowed us to resolve feedbacks between the bivalves and the planktonic ecosystem. We think that one of those feedbacks, the biocapacitor effect, may be responsible for an exponential increase in harvest yield with initial seeding density at low seeding densities.

In this work, we estimated the production carrying capacity of a mussel farm, and we found that the farm in Ship Harbour is currently stocked at approximately half of its carrying capacity. However, we do not recommend to increase the farm's stocking

density because of the large uncertainties associated with the testing of our model in this study (see Section 3.6). We also determined that the estimation of production carrying capacity is sensitive to the natural mortality of bivalves, a parameter that needs to be estimated accurately to produce precise estimations of the production carrying capacity of a system.

Another strength of our hybrid modelling system is that it allows the representation of numerous bivalve ecophysiology variables in a 3-D high-resolution domain. Traditional Eulerian models can only represent a limited number of bivalve variables before the model slows down beyond practical limits. Our hybrid model tracks 20 bivalve ecophysiology variables (3 prognostic and 17 diagnostic). The prognostic variables allow the hybrid model to represent complex physiological processes (e.g. spawning events). The diagnostic variables (e.g. A_k, R_k, $f_k(Temp)$, $f_k(Salt)$, etc.) provide information crucial to the testing of the model (Franks, 2009) and make this model a versatile tool for aquaculture management, particularly when managing multiple size-classes, or multiple species (i.e. polyculture). However, these complex models must be carefully set up with appropriate parameters and rigorously tested against data before their use in operational decision making.

The hybrid model presented in this study is part of the Regional Ocean Modeling System (ROMS), which is an ocean model that has been widely used in applications ranging from effects of climate change (Wang et al., 2008), to larval connectivity (North et al., 2008; Rasmussen et al., 2009), to data assimilation from autonomous underwater vehicles (Chao et al., 2008), and is recognized as state-of-the-art ocean model by the oceanographic community. The use of ROMS for an aquaculture application is a step towards narrowing the gap between fundamental and applied sciences. It is beneficial for the aquaculture community because it adds sound tools to its repertoire, and it is also beneficial for the ocean modelling community because it makes these modelling tools more main-stream and promotes the wide use of these oceanographic techniques.

Acknowledgements

For their insightful comments, we would like to thank Cédric Bacher, Mike Dowd, Marlon Lewis, two anonymous reviewers, and Volker Grimm (Associate Editor). Funding was provided by AquaNet - Canada's Network of Centres of Excellence in Aquaculture, Office of Naval Research, NSERC Discovery, NSERC Research Partnerships, CFCAS, CFI and Dalhousie University.

Appendix A. Supplementary data

Supplementary data associated with this article can be found, in the online version, at http://dx.doi.org/10.1016/j.ecolmodel.2013.10.024.

References

Almada-Villela, P.C., 1984. The effects of reduced salinity on the shell growth of small *Mytilus edulis*. Journal of the Marine Biological Association of the United Kingdom 64, 171–182.

Andresen, H., Dorresteijn, I., van der Meer, J., 2013. Growth and size-dependent loss of newly settled bivalves in two distant regions of the Wadden Sea. Marine Ecology Progress Series 472, 141–154.

Bacher, C., Gangnery, A., 2006. Use of dynamic energy budget and individual based models to simulate the dynamics of cultivated oyster populations. Journal of Sea Research 56, 140–155.

Bacher, C., Grant, J., Hawkins, A.J.S., Fang, J., Zhu, M., Besnard, M., 2003. Modelling the effect of food depletion on scallop growth in Sungo Bay (China). Aquatic Living Resources 16, 10–24.

Bald, J., Sinquin, A., Borja, A., Caill-Milly, N., Duclercq, B., Dang, C., de Montaudouin, X., 2009. A system dynamics model for the management of the Manila clam, *Ruditapes philippinarum* (Adams and Reeve, 1850) in the Bay of Arcachon (France). Ecological Modelling 220, 2828–2837.

Bayne, B.L., Bayne, C.J., Carefoot, T.C., Thompson, R.J., 1976. The physiological ecology of *Mytilus californianus* Conrad. Oecologia 22, 229–250.

Bayne, B.L., Salkeld, P.N., Worrall, C.M., 1983. Reproductive effort and value in different populations of the marine mussel *Mytilus edulis* L. Oecologia 59, 18–26.

Bourles, Y., Alunno-Bruscia, M., Pouvreau, S., Tollu, G., Leguay, D., Arnaud, C., Goulletquer, P., Kooijman, S., 2009. Modelling growth and reproduction of the Pacific oyster *Crassostrea gigas*: advances in the oyster-DEB model through application to a coastal pond. Journal of Sea Research 62, 62–71.

Chao, Y., Li, Z.J., Farrara, J.D., Moline, M.A., Schofield, O.M.E., Majumdar, S.J., 2008. Synergistic applications of autonomous underwater vehicles and regional ocean modeling system in coastal ocean forecasting. Limnology and Oceanography 53, 2251–2263.

Chen, Z., Hu, C., Muller-Karger, F.E., Luther, M.E., 2010. Short-term variability of suspended sediment and phytoplankton in Tampa Bay, Florida: observations from a coastal oceanographic tower and ocean color satellites. Estuarine, Coastal and Shelf Science, 89:62–72.

Cranford, P.J., Hill, P.S., 1999. Seasonal variation in food utilization by the suspension-feeding bivalve molluscs *Mytilus edulis* and *Placopecten magellanicus*. Marine Ecology-Progress Series 190, 223–239.

Dame, R.F., Prins, T.C., 1998. Bivalve carrying capacity in coastal ecosystems. Aquatic Ecology 31, 409–421.

DFO, 2005. BioChem: database of biological and chemical oceanographic data. Version 8. Department of Fisheries and Oceans, Canada. http://www.meds-sdmm.dfo-mpo.gc.ca/biochem/biochem-eng.htm

Dowd, M., 1997. On predicting the growth of cultured bivalves. Ecological Modelling 104, 113–131.

Dowd, M., 2003. Seston dynamics in a tidal inlet with shellfish aquaculture: a model study using tracer equations. Estuarine, Coastal and Shelf Science 57, 523–537.

Dowd, M., 2005. A bio-physical coastal ecosystem model for assessing environmental effects of marine bivalve aquaculture. Ecological Modelling 183, 323–346.

Duarte, P., Fernández-Reiriz, M.J., Filgueira, R., Labarta, U., 2010. Modelling mussel growth in ecosystems with low suspended matter loads. Journal of Sea Research 64, 273–286.

Duarte, P., Labarta, U., Fernandez-Reiriz, M.J., 2008. Modelling local food depletion effects in mussel rafts of Galician Rias. Aquaculture 274, 300–312.

Duarte, P., Meneses, R., Hawkins, A.J.S., Zhu, M., Fang, J., Grant, J., 2003. Mathematical modelling to assess the carrying capacity for multi-species culture within coastal waters. Ecological Modelling 168, 109–143.

FAO, 2010. The state of world fisheries and aquaculture 2010. Rome.

Fennel, K., Wilkin, J., Levin, J., Moisan, J., O'Reilly, J., Haidvogel, D., 2006. Nitrogen cycling in the Middle Atlantic Bight: results from a three-dimensional model and implications for the North Atlantic nitrogen budget. Global Biogeochemical Cycles, 20:GB3007.

Fennel, K., Wilkin, J., Previdi, M., Najjar, R., 2008. Denitrification effects on air-sea CO_2 flux in the coastal ocean: simulations for the northwest North Atlantic. Geophysical Research Letters 35, L24608.

Fennel, K., Hu, J., Laurent, A., Marta-Almeida, M., Hetland, R., 2013. Sensitivity of hypoxia predictions for the Northern Gulf of Mexico to sediment oxygen consumption and model nesting. Journal of Geophysical Research-Oceans 118, 990–1002.

Ferreira, J.G., Hawkins, A.J.S., Monteiro, P., Moore, H., 2008. Integrated assessment of ecosystem-scale carrying capacity in shellfish growing areas. Aquaculture 275, 138–151.

Filgueira, R., Grant, J., Strand Asplin, L., Aure, J., 2010. A simulation model of carrying capacity for mussel culture in a Norwegian fjord: role of induced upwelling. Aquaculture 308, 20–27.

Franks, P.J.S., 2009. Planktonic ecosystem models: perplexing parameterizations and a failure to fail. Journal of Plankton Research 31, 1299–1306.

Fréchette, M., Butman, C.A., Geyer, W.R., 1989. The importance of boundary-layer flows in supplying phytoplankton to the benthic suspension feeder, *Mytilus edulis* L. Limnology and Oceanography 34, 19–36.

Garcia, H.E., Gordon, L.I., 1992. Oxygen solubility in seawater: better fitting equations. Limnology and Oceanography, 1307–1312.

Gonzalez, J.G., Yevich, P., 1976. Responses of an estuarine population of the blue mussel *Mytilus edulis* to heated water from a steam generating plant. Marine Biology 34, 177–189.

Gosling, E.M., 2003. Bivalve molluscs: biology, ecology and culture. Fishing News Books, 443.

Grangeré, K., Lefebvre, S., Bacher, C., Cugier, P., Ménesguen, A., 2010. Modelling the spatial heterogeneity of ecological processes in an intertidal estuarine bay: dynamic interactions between bivalves and phytoplankton. Marine Ecology-Progress Series 415, 141–158.

Grant, J., Bacher, C., Cranford, P.J., Guyondet, T., Carreau, M., 2008. A spatially explicit ecosystem model of seston depletion in dense mussel culture. Journal of Marine Systems 73, 155–168.

Grant, J., Curran, K.J., Guyondet, T.L., Tita, G., Bacher, C., Koutitonsky, V., Dowd, M., 2007. A box model of carrying capacity for suspended mussel aquaculture in Lagune de la Grande-Entree, Iles-de-la-Madeleine, Quebec. Ecological Modelling 200, 193–206.

Gregory, D., Canada Dept. of F. Oceans. Scotia-Fundy Region, P., Chemical Sciences, B. and Bedford Institute of O., 1993. Oceanographic, geographic and hydrological parameters of Scotia-Fundy and southern Gulf of St. Lawrence inlets. Bedford Institute of Oceanography; Department of Fisheries and Oceans, Scotia-Fundy Region, Physical and Chemical Sciences Branch, 248 p.

Grimm, V., Railsback, S.F., 2005. Individual-based Modeling and Ecology. Princeton Univercity Press, New Jersey, USA, pp. 428.

Guyondet, T., Roy, S., Koutitonsky, V.G., Grant, J., Tita, G., 2010. Integrating multiple spatial scales in the carrying capacity assessment of a coastal ecosystem for bivalve aquaculture. Journal of Sea Research 64, 341–359.

Haidvogel, D.B., Arango, H., Budgell, W.P., Cornuelle, B.D., Curchitser, E., Di Lorenzo, E., Fennel, K., Geyer, W.R., Hermann, A.J., Lanerolle, L., Levin, J., McWilliams, J.C., Miller, A.J., Moore, A.M., Powell, T.M., Shchepetkin, A.F., Sherwood, C.R., Signell, R.P., Warner, J.C., Wilkin, J., 2008. Ocean forecasting in terrain-following coordinates: formulation and skill assessment of the Regional Ocean Modeling System. Journal of Computational Physics 227, 3595–3624.

Hall, N.S., Paerl, H.W., 2011. Vertical migration patterns of phytoflagellates in relation to light and nutrient availability in a shallow, microtidal estuary. Marine Ecology-Progress Series 425, 1–19.

Ibarra, D.A., 2003. Estimation of seston depletion by cultured mussels (Mytilus spp.) using measurements of diffuse attenuation of solar irradiance from optical moorings. M.Sc. Thesis, Dalhousie University, Halifax.

Ibarra, D.A., 2011. Interactions between macrobiota (wild and aquacultured) and the physical-planktonic environment: insights from a new 3-D end-to-end modelling framework, Ph.D. Thesis, Dalhousie University, Halifax.

Incze, L.S., Lutz, R.A., True, E., 1981. Modeling carrying capacities for bivalve molluscs in open, suspended-culture systems. Journal of the World Mariculture Society 12, 143–155.

Keizer, P.D., Milligan, T.G., Rao, D.V.S., Strain, P.M., Bugden, G., 1996. Phytoplankton monitoring program: Nova Scotia component - 1989 to 1994. Canadian Technical Report of Fisheries and Aquatic Sciences/Rapport Technique Canadien des Sciences. Halieutiques et Aquatiques 2136, 74.

Koh, C.H., Khim, J.S., Araki, H., Yamanishi, H., Mogi, H., Koga, K., 2006. Tidal resuspension of microphytobenthic chlorophyll a in a Nanaura mudflat, Saga, Ariake Sea, Japan: flood-ebb and spring-neap variations. Marine Ecology-Progress Series 312, 85–100.

Kooijman, S.A.L.M., 1986. Energy budgets can explain body size relations. Journal of Theoretical Biology 121, 269–282.

Kooijman, S.A.L.M., 2000. Dynamic Energy and Mass Budgets in Biological Systems. Cambridge University Press, pp. 424.

Kooijman, S.A.L.M., 2010. Dynamic Energy Budget Theory. Cambridge University Press, Cambridge.

Lande, R., Lewis, M.R., 1989. Models of photoadaptation and photosynthesis by algal cells in a turbulent mixed layer. Deep-Sea Research Part A: Oceanographic Research Papers 36, 1161–1175.

Leon, L.F., Smith, R.E.H., Hipsey, M.R., Bocaniov, S.A., Higgins, S.N., Hecky, R.E., Antenucci, J.P., Imberger, J.A., Guildford, S.J., 2011. Application of a 3D hydrodynamic-biological model for seasonal and spatial dynamics of water quality and phytoplankton in Lake Erie. Journal of Great Lakes Research 37, 41–53.

MacIntyre, H.L., Cullen, J.J., 1996. Primary production by suspended and benthic microalgae in a turbid estuary: time-scales of variability in San Antonio Bay, Texas. Marine Ecology-Progress Series 145, 245–268.

Lotze, H.K., Schramm, W., Schories, D., Worm, B., 1999. Control of macroalgal blooms at early developmental stages: *Pilayella littoralis* versus *Enteromorpha* spp. Oecologia 119, 46–54.

Marinov, D., Galbiati, L., Giordani, G., Viaroli, P., Norro, A., Bencivelli, S., ZaldÃ-var, J.M., 2007. An integrated modelling approach for the management of clam farming in coastal lagoons. Aquaculture 269, 306–320.

McKindsey, C.W., Thetmeyer, H., Landry, T., Silvert, W., 2006. Review of recent carrying capacity models for bivalve culture and recommendations for research and management. Aquaculture 261, 451–462.

Miller, T.J., 2007. Contribution of individual-based coupled physical-biological models to understanding recruitment in marine fish populations. Marine Ecology-Progress Series 347, 127–138.

North, E.W., King, D.M., Xu, J., Hood, R.R., Newell, R.I.E., Paynter, K., Kellogg, M.L., Liddel, M.K., Boesch, D.F., 2010. Linking optimization and ecological models in a decision support tool for oyster restoration and management. Ecological Applications 20, 851–866.

North, E.W., Schlag, Z., Hood, R.R., Li, M., Zhong, L., Gross, T., Kennedy, V.S., 2008. Vertical swimming behavior influences the dispersal of simulated oyster larvae in a coupled particle-tracking and hydrodynamic model of Chesapeake Bay. Marine Ecology-Progress Series 359, 99–115.

Pegau, W.S., Zaneveld, J.R.V., 2000. Field measurements of in-ice radiance. Cold regions Science and Technology 31, 33–46.

Pilditch, C.A., Grant, J., Bryan, K.R., 2001. Seston supply to sea scallops (*Placopecten magellanicus*) in suspended culture. Canadian Journal of Fisheries and Aquatic Sciences 58, 241–253.

Rasmussen, L.L., Cornuelle, B.D., Levin, L.A., Largier, J.L., Di Lorenzo, E., 2009. Effects of small-scale features and local wind forcing on tracer dispersion and estimates of population connectivity in a regional scale circulation model. Journal of Geophysical Research-Oceans 114, C01012.

Rosland, R., Bacher, C., Strand, Å., Aure, J., Strohmeier, T., 2011. Modelling growth variability in longline mussel farms as a function of stocking density and farm design. Journal of Sea Research 66, 318–330.

Rosland, R., Strand, Ø., Alunno-Bruscia, M., Bacher, C., Strohmeier, T., 2009. Applying Dynamic Energy Budget (DEB) theory to simulate growth and bio-energetics of blue mussels under low seston conditions. Journal of Sea Research 62, 49–61.

Sarà, G., Mazzola, A., 2004. The carrying capacity for Mediterranean bivalve suspension feeders: evidence from analysis of food availability and hydrodynamics and their integration into a local model. Ecological Modelling 179, 281–296.

Sarà, G., Palmeri, V., Montalto, V., Rinaldi, A., Widdows, J., 2013. Parameterisation of bivalve functional traits for mechanistic eco-physiological dynamic energy budget (DEB) models. MEPS 480, 99–117.

Sarà, G., Reid, G.K., Rinaldi, A., Palmeri, V., Troell, M., Kooijman, S., 2012. Growth and reproductive simulation of candidate shellfish species at fish cages in the Southern Mediterranean: Dynamic Energy Budget (DEB) modelling for integrated multi-trophic aquaculture. Aquaculture 324, 259–266.

Schulte, E.H., 1975. Influence of algal concentration and temperature on the filtration rate of *Mytilus edulis*. Marine Biology 30, 331–341.

Sénéchal, J., Grant, J., Archambault, M.C., 2008. Experimental manipulation of suspended culture socks: growth and behavior of juvenile mussels (*Mytilus* spp.). Journal of Shellfish Research 27, 811–826.

Smaal, A.C., Vonck, A., 1997. Seasonal variation in C, N and P budgets and tissue composition of the mussel *Mytilus edulis*. Marine Ecology-Progress Series 153, 167–179.

Smith, K.A., North, E.W., Shi, F.Y., Chen, S.N., Hood, R.R., Koch, E.W., Newell, R.I.E., 2009. Modeling the effects of oyster reefs and breakwaters on seagrass growth. Estuaries and Coasts 32, 748–757.

Spillman, C.M., Hamilton, D.P., Hipsey, M.R., Imberger, J., 2008. A spatially resolved model of seasonal variations in phytoplankton and clam (*Tapes philippinarum*) biomass in Barbamarco Lagoon, Italy. Estuarine, Coastal and Shelf Science 79, 187–203.

Strain, P.M., 2002. Nutrient Dynamics in Ship Harbour, Nova Scotia. Atmosphere-Ocean 40, 45–58.

Strickland, J.D.H., Parsons, T.R., 1968. A Practical Handbook of Seawater Analysis. Fisheries Research Board of Canada, Ottawa, pp. 311.

Thompson, R.J., 1984. The reproductive cycle and physiological ecology of the mussel *Mytilus edulis* in a subarctic, non-estuarine environment. Marine Biology 79, 277–288.

Troost, T.A., Wijsman, J.W.M., Saraiva, S., Freitas, V., 2010. Modelling shellfish growth with dynamic energy budget models: an application for cockles and mussels in the Oosterschelde (southwest Netherlands). Philosophical Transactions of the Royal Society B-Biological Sciences 365, 3567–3577.

Wallentinus, I., 1984. Comparisons of nutrient uptake rates for Baltic macroalgae with different thallus morphologies. Marine Biology 80, 215–225.

Wang, S.Y., McGrath, R., Hanafin, J., Lynch, P., Semmler, T., Nolan, P., 2008. The impact of climate change on storm surges over Irish waters. Ocean Modelling 25, 83–94.

Wang, W.X., Widdows, J., 1993. Metabolic responses of the common mussel *Mytilus edulis* to hypoxia and anoxia. Marine Ecology-Progress Series 95, 205.

Warner, J.C., Sherwood, C.R., Signell, R.P., Harris, C.K., Arango, H.G., 2008. Development of a three-dimensional, regional, coupled wave, current, and sediment-transport model. Computers and Geosciences 34, 1284–1306.

Widdows, J., Johnson, D., 1988. Physiological energetics of *Mytilus edulis*: scope for growth. Marine Ecology-Progress Series 46, 113–121.

Winneberger, J.H., Austin, J.H., Klett, C.A., 1963. Membrane filter weight determinations. Journal (Water Pollution Control Federation) 35, 807–813.